Journal of Biomechanics 84 (2019) 94–102

Contents lists available at ScienceDirect

Journal of Biomechanics

journal homepage: www.elsevier.com/locate/jbiomech
www.JBiomech.com

A computationally efficient strategy to estimate muscle forces in a finite element musculoskeletal model of the lower limb

Alessandro Navacchia [a,b,*], Donald R. Hume [a], Paul J. Rullkoetter [a], Kevin B. Shelburne [a]

[a] Dept. of Mechanical and Materials Engineering, The University of Denver, CO, USA
[b] Dept. of Orthopedic Surgery, Mayo Clinic, Rochester, MN, USA

ARTICLE INFO

Article history:
Accepted 12 December 2018

Keywords:
Musculoskeletal modeling
Finite element
Muscle forces
Knee
Multiscale

ABSTRACT

Concurrent multiscale simulation strategies are required in computational biomechanics to study the interdependence between body scales. However, detailed finite element models rarely include muscle recruitment due to the computational burden of both the finite element method and the optimization strategies widely used to estimate muscle forces. The aim of this study was twofold: first, to develop a computationally efficient muscle force prediction strategy based on proportional-integral-derivative (PID) controllers to track gait and chair rise experimental joint motion with a finite element musculoskeletal model of the lower limb, including a deformable knee representation with 12 degrees of freedom; and, second, to demonstrate that the inclusion of joint-level deformability affects muscle force estimation by using two different knee models and comparing muscle forces between the two solutions. The PID control strategy tracked experimental hip, knee, and ankle flexion/extension with root mean square errors below 1°, and estimated muscle, contact and ligament forces in good agreement with previous results and electromyography signals. Differences up to 11% and 20% in the vasti and biceps femoris forces, respectively, were observed between the two knee models, which might be attributed to a combination of differing joint contact geometry, ligament behavior, joint kinematics, and muscle moment arms. The tracking strategy developed in this study addressed the inevitable tradeoff between computational cost and model detail in musculoskeletal simulations and can be used with finite element musculoskeletal models to efficiently estimate the interdependence between muscle forces and tissue deformation.

1. Introduction

Musculoskeletal modeling can provide important insight into body motion and its interaction with the environment, which is of great interest in many fields of science such as medicine, sport, and safety (Pandy, 2001). In particular, musculoskeletal simulations are commonly used to predict muscle forces consistent with experimental motion and external forces collected *in vivo*, providing an estimate of the mechanical environment to which joints/organs are subjected.

For many clinical concerns, such as osteoarthritis, joint replacement, and ligament reconstruction, a multiscale approach to musculoskeletal modeling is needed to examine the essential interactions between movement, muscle forces, and tissue behavior. The current *state of the art* in multiscale modeling consists of a sequential approach: first, a rigid multibody musculoskeletal model at the whole-body level is used to estimate muscle and joint loads, which are subsequently applied as boundary conditions of a second model at the organ/joint level to estimate tissue deformation. For example, This approach has been used to predict ligament and contact forces in the natural knee (Shelburne et al., 2005), patellofemoral (PF) joint stress (Besier et al., 2005), stresses in a total shoulder arthroplasty (Hopkins et al., 2005), bone adaptation in the femur (Geraldes et al., 2015), and knee implant contact mechanics (Navacchia et al., 2016b).

The sequential approach is motivated by the need to select a combination of muscle forces among the infinite possibilities that can produce the same motion. This problem has been routinely solved using optimization techniques that require a large number of evaluations, which are more rapidly performed with simplified representations of muscles and joints (Anderson and Pandy, 2001a; Crowninshield and Brand, 1981). Since muscle forces cannot be directly measured *in vivo*, comparison with measured electromyography (EMG) provides confidence in the plausibility of the

* Corresponding author at: Dept. of Orthopedic Surgery, Mayo Clinic, 200 1st St. SW, Rochester, MN 55905, United States.
E-mail address: Navacchia.Alessandro@mayo.edu (A. Navacchia).

https://doi.org/10.1016/j.jbiomech.2018.12.020
0021-9290/

predicted muscle activations. Alternatively, solutions that use EMG data as inputs to the simulation have been developed to solve the muscle redundancy problem and account for the subject-specific recruitment strategies, but simplified muscles and joints were still used because several evaluations were needed to find optimal muscle parameters or to select the solutions best matching EMG (Lloyd and Besier, 2003; Martelli et al., 2015). As a result, parameters and tissue deformation at the organ/joint level do not influence the selection of muscle forces, as their contribution is assumed to be negligible (small displacement assumption). In principle, models that represent different scales are coupled, and should be solved simultaneously (Viceconti et al., 2006). We previously demonstrated that including a deformable 12-degree-of-freedom knee in a lower limb musculoskeletal model produced significant changes in muscle moment arms during maximum isometric contractions when compared to passive motion (Hume et al., 2018). This finding shows that including joint-level deformation affects muscle parameters, such as moment arm and musculotendon length, which will in turn influence the muscle force needed to produce a specific joint torque. Therefore, predicting muscle forces in a single multiscale framework will include this interdependent action of muscles with subject-specific tissues, such as ligament and cartilage (Tawhai et al., 2009). Concurrent simulations that perform muscle optimization with organ/joint level finite element models have been previously implemented (Ezquerro et al., 2004; Halloran et al., 2009), but the significant increase in computational time due to optimization-based strategies limited model complexity.

Real-time automatic control is a potential alternative to estimate muscle forces based on experimental kinematics and may significantly reduce computational time (Audu and Davy, 1985). More recently, strategies based on conventional proportional-integral-derivative (PID) controllers have been used in a finite element framework to predict muscle forces needed to track *in vivo* knee kinematics (Fitzpatrick et al., 2014). A PID controller minimizes the error between a measure in the model (e.g. knee flexion angle) and an input target profile, generating an input to the model (e.g. muscle force) proportional to the kinematic error, its integral over time, and its rate of change. However, Fitzpatrick et al. (2014) modeled only the quadriceps and hamstrings, representing them as linear actuators without the length and velocity properties of muscle.

The objectives of this investigation were (a) to evaluate the computational advantage of a PID-controller-based strategy to estimate muscle forces in a multiscale model; (b) to verify that muscle activations obtained with this strategy are consistent with measured EMG and, therefore, plausible; and (c) to demonstrate that joint-level deformability affects muscle force estimates when included in a musculoskeletal model. A multiscale finite element musculoskeletal model of the lower limb including a detailed deformable model of the knee and twenty musculotendon units with physiological properties was used (Hume et al., 2018). Muscle-driven forward simulations of chair rise and walking were performed by tracking experimental kinematics measured from two subjects.

2. Methods

Marker-based motion capture, ground reaction forces, and knee radiography were collected for two subjects during chair rise (Subject 1, age 60, 174 cm, 74.8 kg) and gait (Subject 2, age 59, 177.2 cm, 74.4 kg). This study was approved by the University of Denver Institutional Review Board and all participants provided informed consent. Two activities and two subjects were chosen to test the robustness of the muscle control strategy. Dynamic stereo radiographic images were collected at the knee using two matching custom high-speed stereo-radiography (HSSR) systems with 40 cm image intensifiers positioned at a relative angle of 60° (Ivester et al., 2015). Relative tibiofemoral (TF) and PF motion was obtained by optimizing the position of bone geometry models to the two-dimensional radiographs using Autoscoper (XROMM, Brown University, RI) (Miranda et al., 2011). Joint motion at the remaining joints was obtained from the recorded marker locations. Subject 2 kinematics were recorded from 10 to 46% of the gait cycle from contralateral toe-off (CTO) to contralateral heel-strike (CHS).

A finite element musculoskeletal model of the lower limb was created in Abaqus/Explicit (SIMULIA, Providence, RI) (Fig. 1). A detailed description of the musculoskeletal model can be found in Hume et al. (2018). In brief, the model included a 1 degree-of-freedom hinge-joint at the ankle, a 3 degrees-of-freedom ball-joint at the hip, and a 12 degrees-of-freedom joint at the knee. The knee joint included previously described specimen-specific bone and cartilage geometries (femur, tibia and patella), and TF and PF ligaments calibrated to specimen-specific *in vitro* laxity and extension tests (Ali et al., 2016; Harris et al., 2016). To further test the robustness of the tracking strategy, two previously calibrated specimen-specific knee models were implemented in the musculoskeletal model presented here ("S1" and "S2" in Harris et al.). These two knees were chosen because their laxity behavior presented in Harris et al. (2016) showed substantial inter-specimen variability and our goal was to evaluate the impact of different joint models on muscle forces and test the necessity of a multiscale model. Twenty musculotendon units of the lower extremity were represented as one-dimensional connector elements. Some muscles were modeled with via points to represent a non-linear path, while other muscles could wrap around surfaces at the knee, bone, and cartilage geometries. Specifically, the following muscles were included in the model: soleus, gastrocnemius (medialis and lateralis), tibialis anterior, vastus medialis (3 muscu-

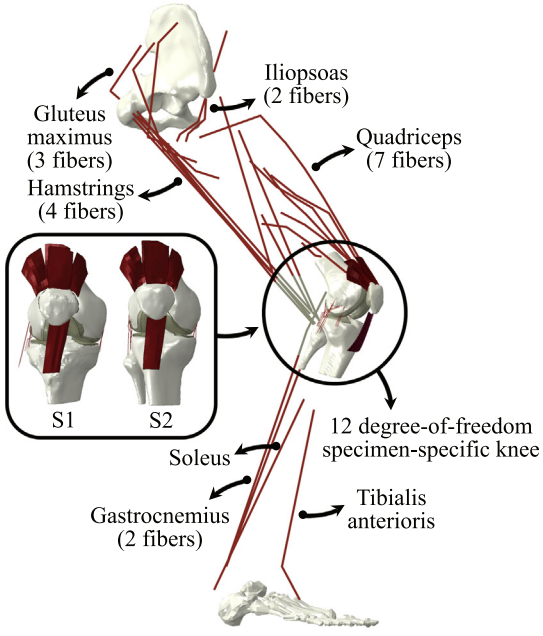

Fig. 1. The lower limb finite element model used in the current study included twenty musculotendon units represented as linear connectors that could generate contraction force. Some muscles were modeled with via points, whereas other muscles could wrap around bone and cartilage surfaces. A 12 degrees-of-freedom knee model was included. Two different specimen-specific knee models (S1 and S2) with TF and PF soft tissue response calibrated on *in vitro* experiments were used (Ali et al., 2016; Harris et al., 2016).

lotendon units), vastus intermedius, vastus lateralis (2 units), rectus femoris, semimembranosus, semitendinosus, biceps femoris short and long head, gluteus maximus (3 units), iliacus and psoas. Each musculotendon unit was modeled as a Hill-type muscle with force-length and force-velocity properties, and with parameters calibrated using maximum isometric extension and flexion torques recorded from healthy subjects (Hume et al., 2018).

A closed-loop strategy was defined to track experimental motion (Fig. 2): three PID controllers were used to track ankle flexion/extension and hip flexion/extension from marker location, and knee flexion/extension from HSSR. The error between target motion and model kinematics was input to the PID controllers to produce muscle activations (see below). The muscles in the model were separated into 6 groups according to their functions: flexors and extensors of ankle, knee and hip. Biarticular muscles belonged to two groups.

A first control step found the activations necessary to hold the model in the initial position of either gait or chair rise with the corresponding ground reaction forces applied at the foot. This first step provided initial activations for a second control step, in which real-time muscle activations were calculated to track the kinematic profiles at the hip, knee, and ankle. Contact between the underside of the foot and ground was not modeled, instead measured ground reaction forces were applied directly to the foot segment at the measured center of pressure. Each PID controlled the motion of one joint providing the change in activation $\Delta a_g(t)$ necessary to the muscle group g to track the reference kinematics:

$$\Delta a_g(t) = k_g^p \cdot e_g(t) + k_g^i \cdot \int_{t_0}^{t} e_g(t)dt + k_g^d \cdot \frac{de_g(t)}{dt} \tag{1}$$

where (k_g^p, k_g^i, k_g^d) is the triplet of PID gains (proportional, integral, and derivative, respectively) for the joint angle controlled by muscle group g, and $e_g(t)$ is the error between model joint angle and target profile. The 6-degree-of-freedom kinematics of the pelvis measured from motion capture was applied to the model. Consequently, the torso was not included, since its contribution was accounted for by the application of ground forces to the foot and the enforced pelvis motion. In summary, the inputs to forward dynamics simulation of each activity were the ground forces applied to the foot, pelvis kinematics, and the activations of the muscles calculated to track sagittal kinematics at the hip, knee, and ankle.

In addition, a recruitment strategy that favors the activation of muscles with larger physiological cross-sectional area (*PCSA*) was employed to reduce muscle stress within each muscle group:

$$\begin{cases} a_m(t) = a_m(t_0) + \Delta a_m(t) = a_m(t_0) + \frac{ng \cdot PCSA_m}{\sum_{i=1}^{ng} PCSA_i} \cdot \Delta a_g(t) \\ 0.02 < a_m(t) < 1.00 \end{cases} \tag{2}$$

where $a_m(t)$ is the activation of muscle m at time t, $\Delta a_g(t)$ is the output of the controller for muscle group g, $a_m(t_0)$ is the initial activation of muscle m calculated in the first control step, ng is the number of muscles belonging to group g, $PCSA_m$ is the *PCSA* of muscle m. *PCSA* has been previously reported to be linearly related to a muscle's maximum force exertion capability (Crowninshield and Brand, 1981) and the proportionality constant represents the maximum stress the muscle can generate. This assumption is commonly adopted in musculoskeletal models that represent musculotendon units as Hill-type models (Anderson and Pandy, 2001a; Delp et al., 1990; Hoy et al., 1990). Therefore, the *PCSA*-based recruitment strategy utilized here has the objective of reducing the overall muscle stress (defined as muscle force divided by *PCSA*), previously linked to muscle endurance (Crowninshield and Brand, 1981).

During an initial tuning process, the gains of the PID controller in Eq. (1) were adjusted to track chair rise kinematics. In a PID controller the proportional and integral gains are responsible for the tracking of the input (throughout the simulation and at steady-state). Therefore, the proportional and integral terms were increased until RMSE between experimental and simulated kinematics smaller than 1° was achieved for each controlled degree-of-freedom. The derivative gain was subsequently adjusted to reduce overshoot in the response without introducing high frequency oscillations. Four simulations were performed with the tuned PID gains: the chair rise of Subject 1 and gait of Subject 2 with both knee models (S1 and S2).

A sensitivity analysis was performed on the chair rise simulation to evaluate how sensitive the results were to changes in PID gains. Six more simulations were run with proportional, integral, and derivative gains increased and decreased by 50%.

Finally, a simulation of chair rise in which the same change in activation $\Delta a_g(t)$ was assigned to all the muscles belonging to the same group (no *PCSA*-based recruitment ratios) was performed to test the impact of the *PCSA* recruitment strategy in Eq. (2):

$$\begin{cases} a_m(t) = a_m(t_0) + \Delta a_g(t) \\ 0.02 < a_m(t) < 1.00 \end{cases} \tag{3}$$

The performance of the two recruitment strategies was compared *a posteriori* with a muscle stress based criterion (Crowninshield and Brand, 1981)

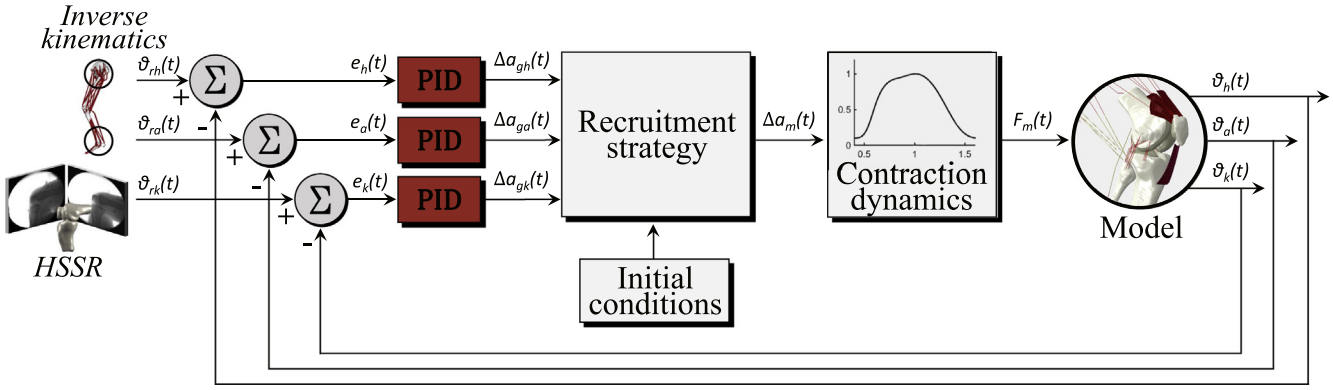

Fig. 2. The closed-loop control system developed in this study consisted of three PID controllers that tracked experimental kinematics from inverse kinematics for hip and ankle, and stereo-radiography for the knee. The error between input and model motion was the input to three controllers, which produced the changes in muscle activation ($\Delta a_g(t)$) needed to follow the target. Changes in activation were scaled according to a recruitment strategy that favored muscles with larger *PCSA*. Muscle forces were calculated with the input activations in Hill-type muscle models, which were applied to the finite element musculoskeletal model. The motion of the model was then forward integrated to the next time step and given back to the error calculation.

$$U(t) = \sqrt[3]{\sum_{i=1}^{n} \left(\frac{F_i(t)}{PCSA_i} \right)^3} \quad (4)$$

where n is the total number of muscles in the model and $F_i(t)$ is the force generated by muscle i at time t.

3. Results

Simulations of chair rise and gait required 76 and 210 min, respectively, using a single Intel® Xeon® 3.60 GHz processor on a desktop computer with 64.0 GB of memory.

The PID gain triplets calibrated for the chair rise simulation were (120-120-2) (k_g^p-k_g^i-k_g^d, respectively) for the hip, (120-120-1) for the knee, and (120-120-0.2) for the ankle. These gains produced RMSE below 1° for both activities and with both S1 and S2 (Fig. 3, Table 1).

Quadriceps forces dominated the chair rise, starting from a peak of 2562/2582 N for S1 and S2, respectively, and decreasing throughout the activity (Fig. 4). Hamstrings and gluteus maximum presented a similar decreasing profile with a combined initial peak of 1704/1749 N for S1/S2. Substantial differences between S1 and S2 were not observed.

The vasti were active during the weight acceptance portion of gait, reaching a peak of 598/534 N (Fig. 4). Soleus and gastrocnemius generated forces during the second part of the stance phase with a combined peak at CHS of 2288/2309 N. The hamstrings muscle that generated the largest force during gait was the biceps femoris short head with a peak of 280/335 N. Peak vasti force was 11% higher and peak biceps femoris short head force was 20% lower for knee S1 than S2.

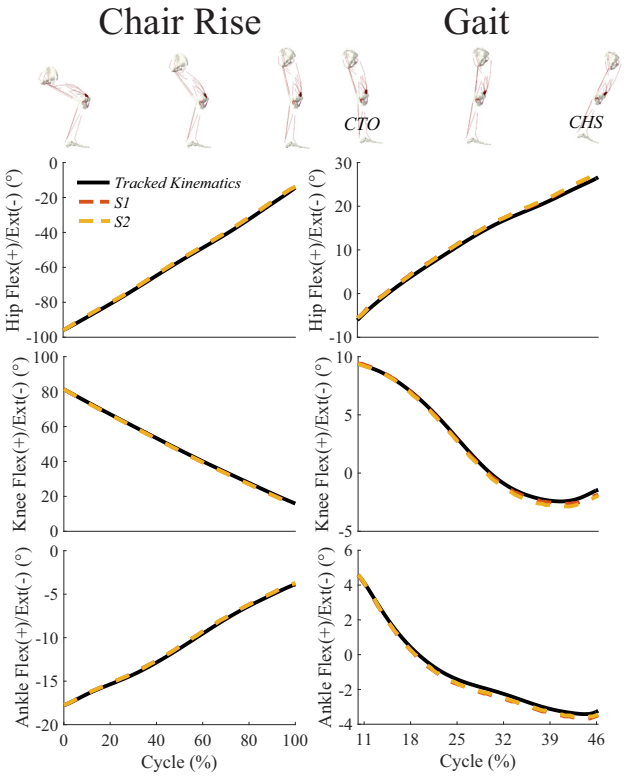

Fig. 3. Hip, knee and ankle flexion/extension kinematics were tracked by three PID controllers to simulate chair rise (left) and gait (right). Tracked kinematics obtained from motion capture (hip and ankle) and stereo-radiography images (knee) is shown with a black solid line. Dashed red and orange lines, which almost overlap, represent model kinematics for the two activities with knees S1 and S2, respectively. All the simulations produced RMSE between tracked motion and model kinematics below 1° using the same PID gains. (For interpretation of the references to colour in this figure legend, the reader is referred to the web version of this article.)

TF compressive forces (along the superior/inferior axis of the tibia) presented a single peak at chair exiting (374/402 %BW) in correspondence with peak quadriceps force (Fig. 5). The lateral side of the tibial plateau bore 70/77% of the peak total force applied to the proximal tibia. PF compressive load presented a decreasing trend with a peak of 309/329 %BW (Fig. 5). The posterior cruciate ligament (PCL) and medial collateral ligament (MCL) provided the highest passive constraint during chair rise for both S1 and S2 with respective peaks of 479/673 N and 429/479 N at chair exit (Fig. 5).

Total compressive force presented an increasing trend during gait from 273/256 %BW at CTO to 386/422 %BW at CHS (Fig. 6). TF compressive load on the lateral compartment of the tibia was on average 14% greater for S2. The patella was in contact with the femur only during weight acceptance with a peak of 32/15 %BW, but not during the second half of the stance phase because of the hyperextension of the knee (Fig. 6). The anterior cruciate ligament (ACL) carried the most load during gait with a peak of 251/249 N at CHS (Fig. 6). PCL and MCL also constrained joint motion with peak forces of 62/49 N (MCL) and 108/32 N (PCL) at maximum knee extension (approximately 38% of the gait cycle) (Fig. 6).

RMSE between model and target kinematics from the sensitivity analysis were below 1° (Table 2). Average RMS differences between baseline muscle forces and forces estimated by the sensitivity analysis simulations peaked at 26.8 N (8% of peak muscle force) (Table 2), and were most sensitive to the proportional term of the PID controller. Muscle stress was higher for the simulation without the *PCSA*-based recruitment strategy throughout the activity cycle (4.3% higher on average).

4. Discussion

A computationally efficient muscle force prediction strategy based on closed-loop kinematics tracking was developed and tested with a finite element multiscale musculoskeletal model of the lower limb. Muscle forces in chair rise and gait were calculated simultaneously with joint level variables, such as contact and ligament forces, in a single forward dynamic simulation. Two different specimen-specific knee models were implemented in the model to investigate differences between predictions and demonstrate the robustness of the tracking strategy.

The main advantage of the tracking strategy presented in this study was that once given a calibrated combination of PID gains for hip, knee and ankle, a single forward integration was required to estimate muscle forces. Previous studies with finite element models of similar complexity that found muscle forces through optimization reported computational times of 10–14 days (Halloran et al., 2010) and 4 weeks (Halloran et al., 2009), mostly due to the large number of iterations required to converge to a solution. A single simulation in the present study was considerably more efficient than methods used with finite element models of similar complexity (76 and 210 min for chair rise and gait, respectively, vs. days or weeks), and in the same order of magnitude of simulations performed with rigid multibody knee models (100 min (Lenhart et al., 2015; Thelen et al., 2014)). Despite being comparable in computational time, the simulations described in Thelen et al. (2014) and Lenhart et al. (2015) required several simplifying assumptions to allow estimation of knee mechanics in a rigid multibody framework, such as constrained motion in knee translational degrees of freedom (Thelen et al., 2014) and minimization of knee secondary kinematic changes between frames

Table 1
RMSE between target kinematics and model motion for hip, knee, and ankle flexion/extension for chair rise and gait simulated with knee models S1 and S2.

	RMSE (°)			
	Chair Rise		Gait	
DoF	S1	S2	S1	S2
Hip	0.58	0.65	0.67	0.68
Knee	0.31	0.36	0.19	0.33
Ankle	0.14	0.14	0.23	0.19

(Lenhart et al., 2015), which limit the realism of simulated joint motion. In contrast, the finite element model presented here can be expanded to include deformable contact, highly nonlinear material properties, and three-dimensional ligaments. The computational efficiency of the tracking strategy allows levels of personalization and deformability that are currently unpractical with optimization-based strategies.

Predicted muscle activations and forces were in good agreement with previous computational studies (Anderson and Pandy, 2001a; Shelburne and Pandy, 2002) and with EMG signals collected for the two subjects (Fig. 4). Anderson and Pandy (2001) also predicted quadriceps force peaking at CTO (~1200 N vs. 966/865 N in this study), and greater forces in the plantarflexor muscles at CHS (~2800 N vs. 2288/2309 N) during gait. Shelburne and Pandy (2002) simulated a rising activity and reported muscle force peaks at ~80° of knee flexion for quadriceps (~2800 N vs. 2562/2582 N), gluteus maximus (~1250 N vs. 992/1036 N) and hamstrings (~600 N vs. 712/713 N).

TF contact force estimates compared favorably to measurements with knee telemetric joint replacements (Bergmann et al., 2014). TF contact loads predicted for chair rise presented a decreasing trend starting from a peak of 374/402 %BW (Fig. 5), which is within two standard deviations of telemetric data from 7 subjects (upper bound: 428 %BW). Load estimates for gait were close to the upper bound of experimental data from 6 subjects reported in Bergmann et al. (2014), but the two peaks at CTO (273/256 %BW) and CHS (386/422 %BW) moderately overpredicted telemetric measurements (Fig. 6). The two typical distinct peaks in TF compressive load during gait were not as evident as in the telemetric data, but this may be motivated by the low extension moment at CTO (~18 Nm) utilized by the test subject. In addition, differences between healthy subjects and those with telemetric implants may be due to dissimilar articular surfaces and ligament behavior.

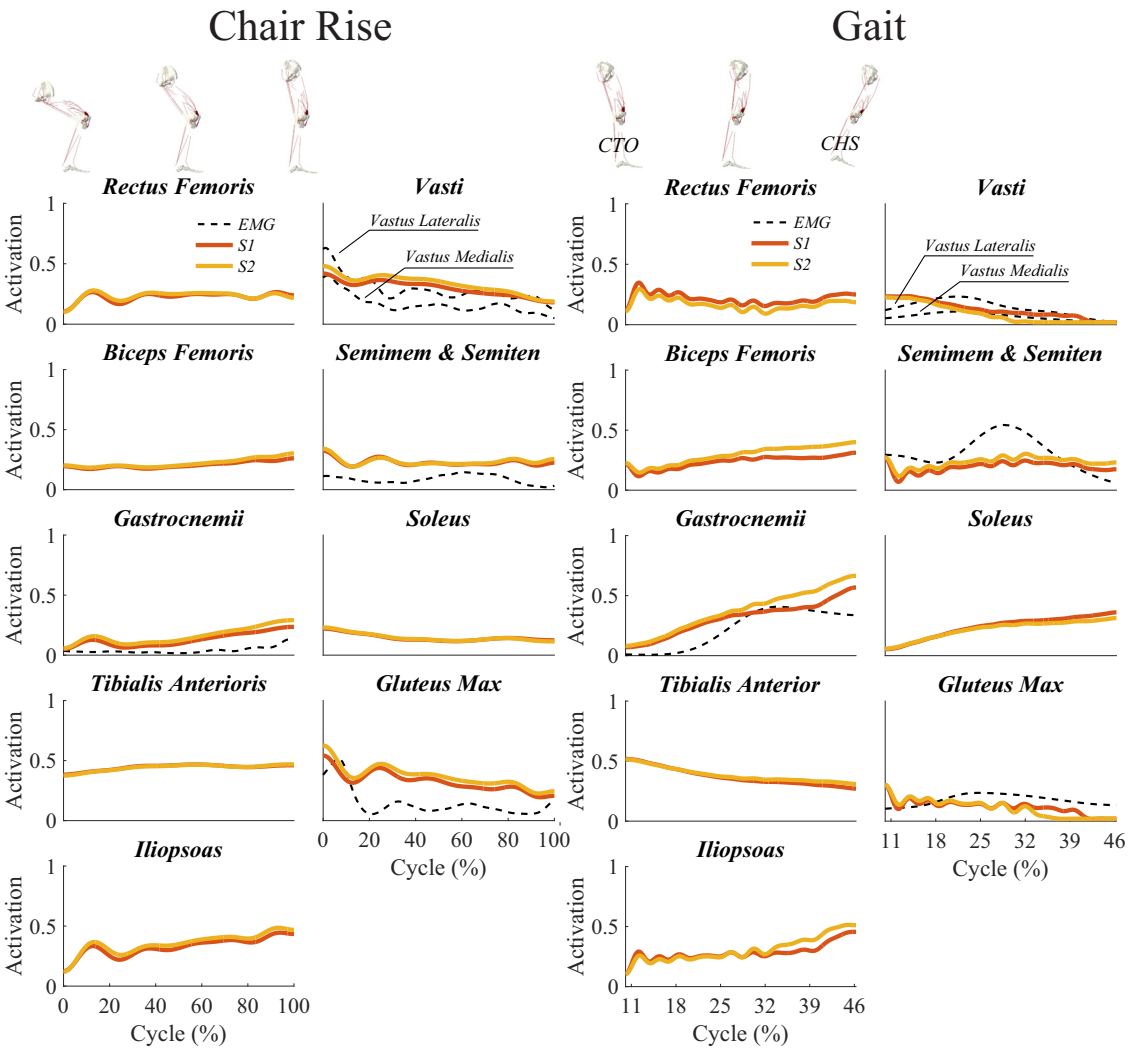

Fig. 4. Muscle activations predicted by the model for chair rise (left) and gait (right). Activation estimates were in good agreement with EMG signals collected for the two subjects (black dashed lines). Quadriceps and gluteus max presented a decreasing trend during chair rise. During gait, the quadriceps was mostly active at CTO, whereas the gastrocnemius and soleus peaked at CHS.

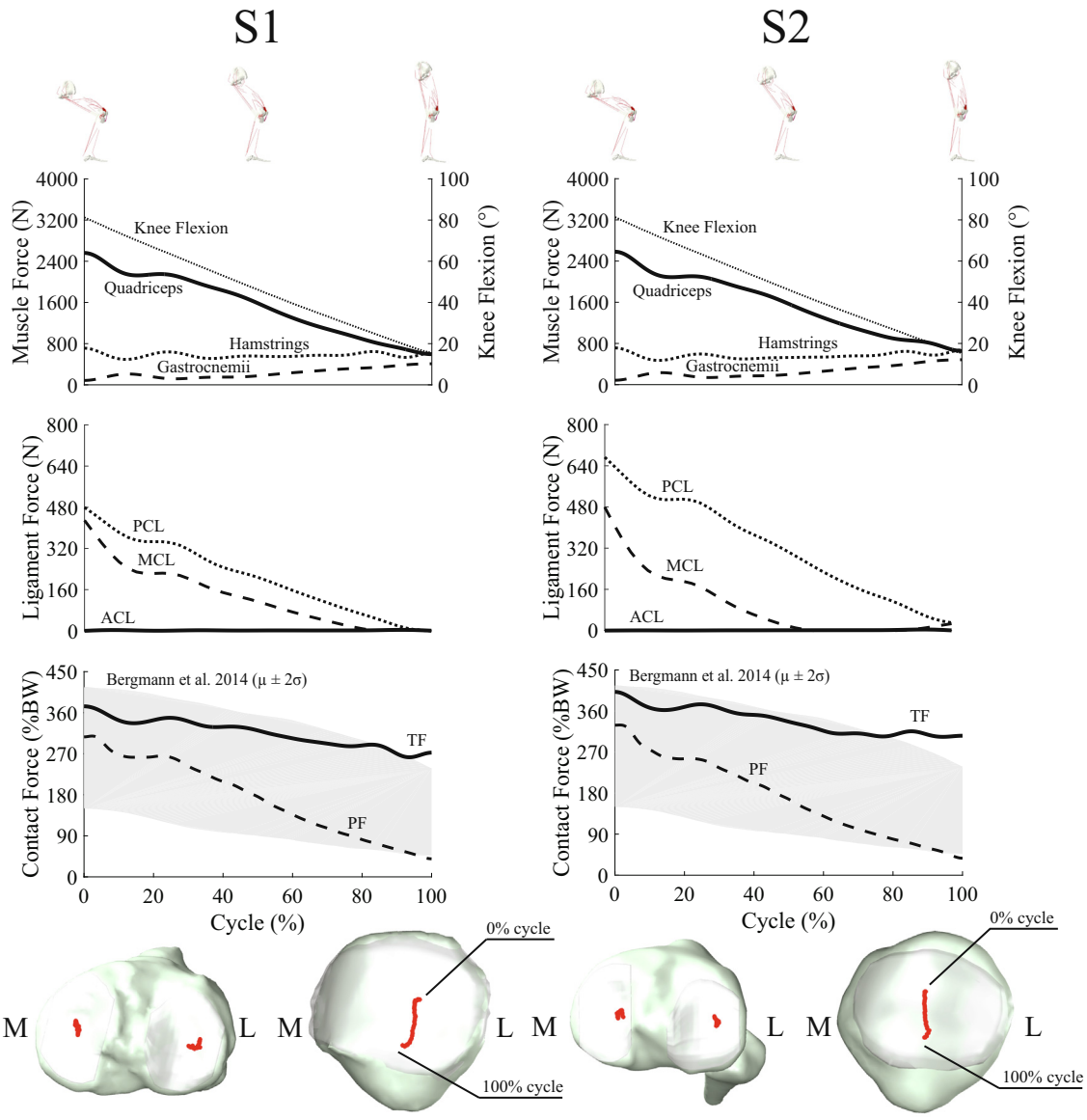

Fig. 5. Muscle, ligament, contact forces, and center of pressure location estimated for chair rise with the two knee models S1 and S2 are presented. Quadriceps forces dominated the chair rise activity and decreased with knee flexion angle. A corresponding decreasing trend was observed for PCL and MCL forces, and TF and PF compressive loads. Center of pressure for the PF joint started on the superior part of the patella at higher flexion angles (~80°) and moved to the inferior part throughout the chair rise. The results obtained with the two knee models presented similar trends, but some differences were also observed. Peak PCL forces were 40% larger for S2. Similar trends were observed for the center of pressure on the patella, but S2 presented a more medial contact location in comparison to S1.

The magnitude and trend of ligament forces agreed with estimates from previously published data. As observed in the present study (Fig. 6), Shelburne and Pandy (2002) estimated PCL force peaking in deep knee flexion (~660 N at 80° of flexion) and turning off at 30°. ACL was most prominent during gait with a smaller peak at CTO observed only for S1 (73 N), and a larger peak at CHS observed for both knees (251/249 N). While the first peak is supported by results previously reported (Harrington, 1976; Shelburne et al., 2004), the second peak might be explained by the hyperextension of the knee measured from Subject 2 in late stance (Fig. 3).

Differences between the muscle, joint, and ligament forces estimated with the two knee models were observed. Specifically, peak quadriceps and hamstrings forces for S1 were 10% higher and 10% lower than for S2, respectively. TF and PF contact forces were also influenced by the knee model, presenting different distributions on the tibial plateaus and different peaks. Since the same anthropometry, external forces and kinematics were used for the two models, these changes in muscle forces were attributed to the differences between the two specimen-specific knees. A combination of differing joint contact geometry (Smoger et al., 2015), ligament behavior (Smith et al., 2016), joint kinematics (Navacchia et al., 2017), and muscle properties (Hume et al., 2018; Navacchia et al., 2016a) may have produced this effect. Therefore, although differences in muscle forces were small (~10%), they demonstrated our hypothesis that joint-scale properties affect muscle forces, confirming that joint mechanics should be estimated concurrently. This bidirectional interdependence (muscle to joint, and joint to muscle) might be crucial for clinical investigations that require a multiscale approach, such as ligament injury, anterior knee pain, and total joint replacement (Tawhai et al., 2009).

The tracking strategy presented here has the primary objective of reducing computational time, with limited implications on the actual mechanism underlying neuromuscular recruitment. Muscu-

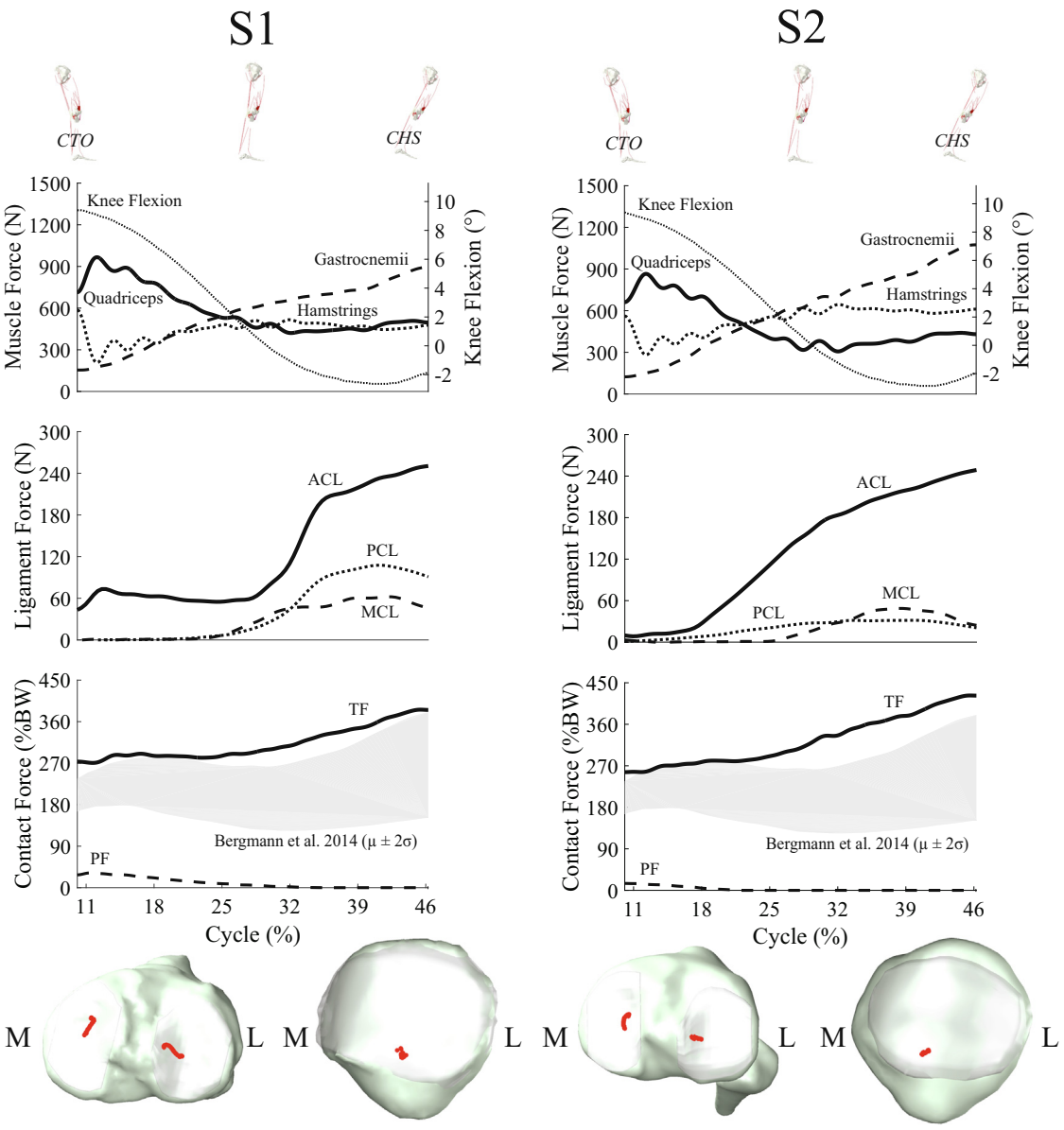

Fig. 6. Muscle, ligament, contact forces, and center of pressure location estimated for gait with the two knee models S1 and S2 are presented. The quadriceps peaked at CTO, while the gastrocnemius peaked at CHS. ACL, PCL, and MCL carried load during the second half of the stance phase, when the knee hyperextended. The results obtained with the two knee models present similar trends, but some differences were also observed. The ACL of the S2 knee did not carry any load at CTO, unlike S1. Peak PCL forces were 70% smaller for S2. S2 presented a more medial contact location in comparison to S1.

Table 2
Sensitivity analysis results. RMSE between target kinematics and model motion for hip, knee, and ankle flexion/extension for chair rise simulated with knee model S1 are shown on top. Baseline indicates the simulation that used baseline PID gains (see text for details). P+ = Proportional gains + 50%; P– = Proportional gains –50%; I+ = Integral gains + 50%; I– = Integral gains –50%; D+ = Derivative gains + 50%; D– = Derivative gains –50%. Average RMS differences between muscle forces predicted with baseline PID gains and with the sensitivity analysis simulations are shown on the bottom. RMS differences are expressed both in N and in % of the peak force for each muscle.

DoF	Baseline	P+	P–	I+	I–	D+	D–
RMSE (°)							
Hip	0.58	0.44	0.91	0.51	0.69	0.58	0.60
Knee	0.31	0.23	0.48	0.27	0.36	0.31	0.32
Ankle	0.14	0.10	0.21	0.12	0.16	0.14	0.14
Average RMS difference							
Muscle forces	–	26.8 N 8.1%	22.2 N 6.8%	1.6 N 0.5%	1.6 N 0.5%	8.8 N 2.7%	10.4 N 3.1%

loskeletal simulations have implemented optimal recruitment strategies to solve the muscle redundancy problem, trying to emulate the criteria that drive neuromuscular activation selection, and obtained satisfying results simulating healthy gait (Anderson and Pandy, 2001a, b). However, good evidence indicates that our nervous system does not use an internal model to optimally select

muscles. Neuromuscular recruitment does not track desired kinematics with optimal control but aims to satisfy competing goals with a habitual 'sub-optimal' strategy (Loeb, 2012), selecting from a manifold of possible solutions (Scholz and Schoner, 1999). Consequently, alternative solutions based on EMG measurements have accounted for subject-specific muscle recruitment strategies (Lloyd and Besier, 2003; Martelli et al., 2015). The actual neuromuscular control strategies adopted by the central nervous system remain unclear and are the object of ongoing research. The main objective of the current musculoskeletal simulations of movement were to estimate a realistic loading environment, while addressing the inevitable tradeoff between computational efficiency and model detail and providing evidence that joint-scale properties can partially alter predicted muscle forces, requiring a concurrent multiscale simulation approach.

A number of limitations were present in this study. First, the knee models used in this study did not represent the geometry and properties of the knees of the two subjects. This limiting factor might have influenced ligament and contact predictions. However, although ligament geometry may be determined by MRI, reliable techniques to measure the interaction between knee laxity and ligament properties *in vivo* are currently not available. The priority of this study was to include realistic knee properties to evaluate the robustness of the muscle control strategy to changes in model representations. Therefore, we chose to use models of the healthy knee that had been subjected to rigorous calibration and validation in prior work (Ali et al., 2016; Harris et al., 2016). An additional limitation was that the computational cost of each simulation depended on the complexity of the model. For example, the inclusion of deformable contact and three-dimensional ligaments would potentially increase simulation time. However, the substantial reduction in computational time compared to optimization methods with previously presented finite element models (Halloran et al., 2010) will allow practical solution of the redundancy problem in reasonable simulation times despite a potential increase in model complexity. In addition, the tracking strategy recruited muscle groups according to their function, rather than single muscles, preventing substantial differences between activation trends of muscles belonging to the same group(s). Using *PCSA* to distribute force approximates what occurs *in vivo* and may not accurately represent actual force distribution. However, this approach produced results that were similar to prior results obtained by minimizing muscles stress, which is a common performance criterion in musculoskeletal simulation (Anderson and Pandy, 2001b; Crowninshield and Brand, 1981). In future work, the control loop strategy might be expanded to track experimentally measured EMG data, providing more differentiation between agonist muscles.

A computationally efficient muscle prediction strategy was developed to perform muscle-driven forward-dynamic simulations of gait and chair rise with a finite element musculoskeletal model of the lower limb. The muscle prediction strategy was robust to changes in knee model and in simulated activity, since the same PID gains produced RMSE under 1° for both activities and with both knee models, and with low sensitivity to changes in PID gains. These results gave confidence that the gains will not require frequent tuning for similar activities and additional knee models. Additionally, the similarity between results presented in this study and previous investigations suggests that our strategy is a viable alternative to computationally expensive optimization-based approaches, which are prohibitive with complex deformable representations. A multiscale musculoskeletal model that includes a detailed knee representation can address clinical questions that require investigating the interaction between pathological conditions at the joint and the neuromuscular system.

Acknowledgements

Supported in part by the NIH National Institute of Biomedical Imaging and Bioengineering R01 EB015497.

Conflict of interest statement

The authors declared that there is no conflict of interest.

References

Ali, A.A., Shalhoub, S.S., Cyr, A.J., Fitzpatrick, C.K., Maletsky, L.P., Rullkoetter, P.J., Shelburne, K.B., 2016. Validation of predicted patellofemoral mechanics in a finite element model of the healthy and cruciate-deficient knee. J. Biomech. 49, 302–309.
Anderson, F.C., Pandy, M.G., 2001a. Dynamic optimization of human walking. J. Biomech. Eng. 123, 381–390.
Anderson, F.C., Pandy, M.G., 2001b. Static and dynamic optimization solutions for gait are practically equivalent. J. Biomech. 34, 153–161.
Audu, M.L., Davy, D.T., 1985. The influence of muscle model complexity in musculoskeletal motion modeling. J. Biomech. Eng. 107, 147–157.
Bergmann, G., Bender, A., Graichen, F., Dymke, J., Rohlmann, A., Trepczynski, A., Heller, M.O., Kutzner, I., 2014. Standardized loads acting in knee implants. PloS One 9, e86035.
Besier, T.F., Gold, G.E., Beaupre, G.S., Delp, S.L., 2005. A modeling framework to estimate patellofemoral joint cartilage stress in vivo. Med. Sci. Sports Exerc. 37, 1924–1930.
Crowninshield, R.D., Brand, R.A., 1981. A physiologically based criterion of muscle force prediction in locomotion. J. Biomech. 14, 793–801.
Delp, S.L., Loan, J.P., Hoy, M.G., Zajac, F.E., Topp, E.L., Rosen, J.M., 1990. An interactive graphics-based model of the lower extremity to study orthopaedic surgical procedures. IEEE Trans. Biomed. Eng. 37, 757–767.
Ezquerro, F., Simon, A., Prado, M., Perez, A., 2004. Combination of finite element modeling and optimization for the study of lumbar spine biomechanics considering the 3D thorax-pelvis orientation. Med. Eng. Phys. 26, 11–22.
Fitzpatrick, C.K., Baldwin, M.A., Clary, C.W., Maletsky, L.P., Rullkoetter, P.J., 2014. Evaluating knee replacement mechanics during ADL with PID-controlled dynamic finite element analysis. Comput. Methods Biomech. Biomed. Eng. 17, 360–369.
Geraldes, D.M., Modenese, L., Phillips, A.T., 2015. Consideration of multiple load cases is critical in modelling orthotropic bone adaptation in the femur. Biomech. Model. Mechanobiol.
Halloran, J.P., Ackermann, M., Erdemir, A., van den Bogert, A.J., 2010. Concurrent musculoskeletal dynamics and finite element analysis predicts altered gait patterns to reduce foot tissue loading. J. Biomech. 43, 2810–2815.
Halloran, J.P., Erdemir, A., van den Bogert, A.J., 2009. Adaptive surrogate modeling for efficient coupling of musculoskeletal control and tissue deformation models. J. Biomech. Eng 131, 011014.
Harrington, I.J., 1976. A bioengineering analysis of force actions at the knee in normal and pathological gait. Biomed. Eng. 11, 167–172.
Harris, M.D., Cyr, A.J., Ali, A.A., Fitzpatrick, C.K., Rullkoetter, P.J., Maletsky, L.P., Shelburne, K.B., 2016. A combined experimental and computational approach to subject-specific analysis of knee joint laxity. J. Biomech. Eng. 138..
Hopkins, A.R., Hansen, U.N., Amis, A.A., 2005. Finite element models of total shoulder replacement: application of boundary conditions. Comput. Methods Biomech. Biomed. Eng. 8, 39–44.
Hoy, M.G., Zajac, F.E., Gordon, M.E., 1990. A musculoskeletal model of the human lower extremity: the effect of muscle, tendon, and moment arm on the moment-angle relationship of musculotendon actuators at the hip, knee, and ankle. J. Biomech. 23, 157–169.
Hume, D.R., Navacchia, A., Ali, A.A., Shelburne, K.B., 2018. The interaction of muscle moment arm, knee laxity, and torque in a multi-scale musculoskeletal model of the lower limb. J. Biomech. 76, 173–180.
Ivester, J.C., Cyr, A.J., Harris, M.D., Kulis, M.J., Rullkoetter, P.J., Shelburne, K.B., 2015. A reconfigurable high-speed stereo-radiography system for sub-millimeter measurement of in vivo joint kinematics. J. Med. Devices 9, 041009.
Lenhart, R.L., Kaiser, J., Smith, C.R., Thelen, D.G., 2015. Prediction and validation of load-dependent behavior of the tibiofemoral and patellofemoral joints during movement. Ann. Biomed. Eng. 43, 2675–2685.
Lloyd, D.G., Besier, T.F., 2003. An EMG-driven musculoskeletal model to estimate muscle forces and knee joint moments in vivo. J. Biomech. 36, 765–776.
Loeb, G.E., 2012. Optimal isn't good enough. Biol. Cybern. 106, 757–765.
Martelli, S., Calvetti, D., Somersalo, E., Viceconti, M., 2015. Stochastic modelling of muscle recruitment during activity. Interface Focus, 5.
Miranda, D.L., Schwartz, J.B., Loomis, A.C., Brainerd, E.L., Fleming, B.C., Crisco, J.J., 2011. Static and dynamic error of a biplanar videoradiography system using marker-based and markerless tracking techniques. J. Biomech. Eng. 133, 121002.
Navacchia, A., Kefala, V., Shelburne, K.B., 2017. Dependence of muscle moment arms on in vivo three-dimensional kinematics of the knee. Ann. Biomed. Eng. 45, 789–798.

Navacchia, A., Myers, C.A., Rullkoetter, P.J., Shelburne, K.B., 2016a. Prediction of in vivo knee joint loads using a global probabilistic analysis. J. Biomech. Eng 138, 4032379.
Navacchia, A., Rullkoetter, P.J., Schutz, P., List, R.B., Fitzpatrick, C.K., Shelburne, K.B., 2016b. Subject-specific modeling of muscle force and knee contact in total knee arthroplasty. J. Orthop. Res.
Pandy, M.G., 2001. Computer modeling and simulation of human movement. Annu. Rev. Biomed. Eng. 3, 245–273.
Scholz, J.P., Schoner, G., 1999. The uncontrolled manifold concept: identifying control variables for a functional task. Exp. Brain Res. 126, 289–306.
Shelburne, K.B., Pandy, M.G., 2002. A dynamic model of the knee and lower limb for simulating rising movements. Comput. Methods Biomech. Biomed. Eng. 5, 149–159.
Shelburne, K.B., Pandy, M.G., Anderson, F.C., Torry, M.R., 2004. Pattern of anterior cruciate ligament force in normal walking. J. Biomech. 37, 797–805.
Shelburne, K.B., Torry, M.R., Pandy, M.G., 2005. Muscle, ligament, and joint-contact forces at the knee during walking. Med. Sci. Sports Exerc. 37, 1948–1956.
Smith, C.R., Lenhart, R.L., Kaiser, J., Vignos, M.F., Thelen, D.G., 2016. Influence of ligament properties on tibiofemoral mechanics in walking. J. Knee Surg. 29, 99–106.
Smoger, L.M., Fitzpatrick, C.K., Clary, C.W., Cyr, A.J., Maletsky, L.P., Rullkoetter, P.J., Laz, P.J., 2015. Statistical modeling to characterize relationships between knee anatomy and kinematics. J. Orthop. Res. 33, 1620–1630.
Tawhai, M., Bischoff, J., Einstein, D., Erdemir, A., Guess, T., Reinbolt, J., 2009. Multiscale modeling in computational biomechanics. IEEE Eng. Med. Biol. Mag. 28, 41–49.
Thelen, D.G., Won Choi, K., Schmitz, A.M., 2014. Co-simulation of neuromuscular dynamics and knee mechanics during human walking. J. Biomech. Eng. 136, 021033.
Viceconti, M., Testi, D., Taddei, F., Martelli, S., Clapworthy, G.J., Jan, S.V.S., 2006. Biomechanics modeling of the musculoskeletal apparatus: status and key issues. Proc. IEEE 94, 725.